Materials Science in Semiconductor Processing 27 (2014) 966–974

Contents lists available at ScienceDirect

Materials Science in Semiconductor Processing

journal homepage: www.elsevier.com/locate/mssp

Visible-light enhancement of methylene blue photodegradation by graphitic carbon nitride-titania composites

Dongying Fu, Gaoyi Han*, Feifei Liu, Yaoming Xiao, Hongfei Wang, Ruiqin Liu, Cuixian Liu

Institute of Molecular Science, Key Laboratory of Chemical Biology and Molecular Engineering of the Ministry of Education, Shanxi University, Taiyuan 030006, PR China

ARTICLE INFO

Available online 19 September 2014

Keywords:
g-C_3N_4
TiO_2
Melamine
Photocatalytic degradation
Methylene blue
Visible light

ABSTRACT

Composites of graphite-like C_3N_4 (g-C_3N_4) and TiO_2 were synthesized by direct heating of melamine in the presence of different TiO_2 amounts in a semi-closed stainless steel container. The resulting samples were characterized using X-ray diffraction, X-ray photoelectron spectroscopy (XPS), UV-visible diffuse reflectance spectroscopy (DRS), photoluminescence spectrum (PLS), thermogravimetric analysis, scanning electron microscopy, and transmission electron microscopy techniques. The results reveal that the microstructure and DRS and PLS characteristics of the composites vary with the composition. XPS Ti 2p peaks for the composites exhibit a shift to lower binding energy in comparison to pure TiO_2. The photocatalytic degradation properties of the composites were evaluated using methylene blue (MB) as a model compound under visible light irradiation (400–600 nm). The results indicate that photocatalytic degradation of MB is higher for g-C_3N_4–TiO_2 composites with optimum TiO_2 content (26.4 and 80.0 wt%) than for pure g-C_3N_4 or TiO_2. Moreover, the activity of an optimum composite sample was still as high as 91% after use in four consecutive photocatalytic cycles.

1. Introduction

Over the past few decades, photocatalysis has been considered as a very promising technique for hydrogen production and removal of environmental pollutants [1–4]. Among metal oxide photocatalysts, TiO_2 has attracted much attention because of its low cost, low toxicity, photochemical stability, high photocatalytic activity, and biocompatibility [5–7]. However, the bandgap of TiO_2 is 3.0 eV for the rutile phase and 3.2 eV for the anatase phase, so UV radiation is required for activation and relatively little of the solar spectral range (4–5%) is used [8]. Therefore, the main focus of recent research into TiO_2 photocatalysis has been on how to improve the catalytic activity under visible light irradiation. There have been substantial attempts to induce absorption of visible light by TiO_2 for effective utilization of solar energy and improved separation of photogenerated electrons and holes. For instance, Moon et al. improved the visible-light photocatalytic activity of TiO_2 using acid red 44 as a modifier [9]. Asahi et al. investigated photocatalysis by nitrogen-doped titanium oxides under visible light [10]. Enhancement of photodegradation efficiency using Pt–TiO_2 catalysts [11] and B_2O_3–SiO_2–TiO_2 ternary mixed oxides [12] has also been investigated and the results revealed that these composites exhibit higher photocatalytic activity when compared with TiO_2. However, there is still a need to develop novel TiO_2-based composites to improve the activity of TiO_2 under visible light.

* Corresponding author. Tel.: +86 351 7010699; fax: +86 351 7016358.
E-mail address: han_gaoyis@sxu.edu.cn (G. Han).

http://dx.doi.org/10.1016/j.mssp.2014.08.004
1369-8001/

Graphite-like C_3N_4 (g-C_3N_4) is a novel and metal-free photocatalyst with a conjugated π structure that absorbs visible light [13–15] and it has been used as a catalyst in several reactions [16,17]. Moreover, it is inexpensive, environmentally benign, and can be easily prepared via numerous facile methods [18,19]. However, the efficiency of pure g-C_3N_4 is limited owing to recombination of photogenerated electron–hole pairs because of its narrow bandgap energy (2.7 eV). Various strategies such as doping with metal or nonmetal species [20–22], sensitization with organic dyes [23], and coupling with other semiconductors [24] have been adopted to improve the photocatalytic performance of g-C_3N_4. Several recent reports on application of g-C_3N_4–TiO_2 in photocatalysis describe the synthesis of g-C_3N_4 and then g-C_3N_4–TiO_2. For example, a g-C_3N_4–TiO_2 composite containing 66.7% g-C_3N_4 with good photocatalytic activity was synthesized hydrolytically using g-C_3N_4 as a support [25]. Miranda et al. synthesized g-C_3N_4–TiO_2 containing 2 wt% g-C_3N_4 via an impregnation method [26]. Lu et al. prepared a g-C_3N_4–TiO_2 composite by combining sol–gel and hydrothermal methods [27]. Yang et al. synthesized an N-doped TiO_2–C_3N_4 composite by heating a mixture of the hydrolysis product of $TiCl_4$ and g-C_3N_4 [28]. A TiO_2–g-C_3N_4 composite was also prepared by ball-milling of TiO_2 and g-C_3N_4 powder and the product was heated at 400 °C for 1 h and used in photocatalytic production of H_2 under visible light irradiation [29]. According to the above studies, the g-C_3N_4 sheet size does not change during composite synthesis because g-C_3N_4 is synthesized first. However, g-C_3N_4 synthesis has some disadvantages, such as low yield and difficulty in controlling the quality because of sublimation of the precursor (e.g. melamine) during pyrolysis.

To the best of our knowledge, preparation methods for composites containing g-C_3N_4 mostly involve mixing of other components with prepared g-C_3N_4 and some subsequent treatment [26,27]. In most cases, the composite is g-C_3N_4-modified TiO_2 or TiO_2-modified g-C_3N_4 and the properties of a composite with one main component are investigated [30,31]. Because both TiO_2 and g-C_3N_4 are semiconductors, the two components can be used as modifiers for each other. In the present study, we synthesized g-C_3N_4–TiO_2 composites by directly heating melamine and TiO_2 in a semi-closed system. This new and facile approach can be used to prepare pure g-C_3N_4 in high yield of 95%. The preparation of g-C_3N_4–TiO_2 via thermal treatment of a mixture of TiO_2 and melamine is reported for the first time. Compared with pure g-C_3N_4 and TiO_2, the optimum g-C_3N_4–TiO_2 composite exhibits enhanced activity for photocatalytic degradation of methylene blue (MB) under visible light irradiation.

2. Experimental

2.1. Materials

TiO_2 (P25) was obtained from the Guangzhou Kosin (Evonik Degussa). Melamine was purchased from Aladdin Chemistry. Other chemicals were of analytical reagent grade and were used without further purification. MB was obtained from Zhangjiagang Chemical Plant. Deionized water was used in all experiments.

2.2. Synthesis of g-C_3N_4

g-C_3N_4 was obtained by pyrolysis of melamine powder. In brief, 1.0 g of melamine was poured into a cylindrical stainless steel container (Fig. S1) after it was fully ground in an agate mortar. The container was sealed with a screw-on lid and transferred to a muffle furnace. The temperature was increased at 3.0 °C min^{-1} and samples were heated at temperatures ranging from 500 °C to 560 °C for 4 h. After cooling to room temperature, the resultant yellow solid (Fig. S2) was milled into powder and collected (yield ~95%).

2.3. Fabrication of g-C_3N_4–TiO_2 composites

To prepare g-C_3N_4–TiO_2 composites, a certain amount of melamine (1.0 g) was mixed with different amounts of TiO_2 powder. The mixture was ground thoroughly in an agate mortar and poured into a cylindrical stainless steel container, which was then sealed with a screw-on lid. Mixtures of different composition were heated in a muffle furnace at different temperatures (500–560 °C) for 4 h at a heating rate of 3.0 °C min^{-1}. g-C_3N_4–TiO_2 composites prepared at 540 °C containing 9.2, 16.1, 26.4, 46.9, 69.3, 80.0, and 89.1 wt% TiO_2 are denoted as g-C_3N_4–TiO_2-9, -16, -26, -47, -69, -80, and -89, respectively.

2.4. Characterization

X-Ray photoelectron spectroscopy (XPS) measurements were performed on an Axis Ultra DLD spectrometer (Kratos Shimadzu) using a monochromic Al K_α source at 1486.6 eV, with power of 150 W for a sample analysis area of approximately 700 μm × 300 μm. X-Ray diffraction (XRD) patterns of the samples were recorded on a Bruker D8 Advance X-ray diffractometer with Cu K_α radiation and a graphite monochromator. The scan speed was 5° min^{-1} and the step size was 0.02°. The sample morphology was observed using a Jeol JSM-6701 field-emission scanning electron microscope (SEM) operating at an accelerating voltage of 10 kV and a Jeol 2010 transmission electron microscopy (TEM) operating at 200 kV. UV-Vis diffuse reflectance spectra (DRS) were recorded on a Thermo Scientific Evolution 220 UV-visible spectrophotometer. The fluorescence properties of the samples were investigated using a Hitachi F-2500 spectrofluorimeter at room temperature. The MB spectral absorbance during photodegradation was measured on a Varian 50 Bio UV-visible spectrophotometer. Thermogravimetric analysis (TGA) was performed on a STA449C thermogravimetric analyzer from room temperature to 800 °C at a heating rate of 10 °C min^{-1}.

2.5. Photodegradation measurements

Photocatalytic experiments were carried out using MB in solution as a model compound. In a typical run, 50.0 mL of MB solution (20.0 mg L^{-1}) containing a certain amount of photocatalyst in a 100-mL beaker was stirred for 30 min in

the dark under ambient conditions to achieve absorption–desorption equilibrium before irradiation. The visible light (400–600 nm) used for photocatalytic degradation was generated by a 200-W Xe lamp equipped with a UV cutoff filter. For irradiation, the lamp was positioned 36 cm away from the sample beaker. The photocatalytic reaction was initiated by turning on the Xe lamp. During photocatalysis, MB degradation was monitored by measuring the UV absorbance at given time intervals. During photodegradation, the temperature was kept at ~25 °C and the pH at ~7.0. At given time intervals, 1.0 mL of the solution was removed and centrifuged at 12,000 rpm for 10 min to precipitate the catalyst particles. The absorbance of the solution was measured in an ethanol/water mixture (3:1 v/v). Control experiments, which included irradiation without a photocatalyst and no irradiation in the presence of a photocatalyst, were carried out using the same procedure. The solution pH was adjusted using HCl and NaOH solutions. Catalyst stability for MB photodegradation was also tested using the same procedure. A 30.0-mg of photocatalyst was initially dispersed in 50.0 mL of MB solution (20.0 mg L^{-1}) and the same photocatalyst sample was used in four consecutive cycles, each lasting for 3 h. After each cycle, the catalyst was centrifuged, washed thoroughly with water, and then added to fresh MB solution.

3. Results and discussion

3.1. Characterization

Fig. 1a shows XRD patterns for g-C_3N_4 synthesized at different temperatures. It is evident that g-C_3N_4 was successfully synthesized at ≥520 °C, while an oligomer is the main product at 500 °C. The g-C_3N_4 samples prepared at 540 °C and 560 °C show two distinct peaks at 13.1° and 27.4° corresponding to the characteristic in-plane structural arrangement parallel to the *c*-axis and the long-range interplanar stacking of aromatic systems, respectively [32,33]. The g-C_3N_4 size calculated using the (002) peak is ~7.2 nm. However, no shift of the (002) peak to higher angle was observed with increasing temperature, in contrast to previous studies [26,34], which indicates that the interplanar stacking distance does not change at higher condensation temperatures such as 560 °C. The XRD pattern for TiO_2 reveals that it contains mainly anatase phase and little rutile phase (Fig. 1b, curve d). The XRD patterns for g-C_3N_4–TiO_2-26 and g-C_3N_4–TiO_2-80 (Fig. 1b, curves b and c) exhibit the characteristics of both g-C_3N_4 and TiO_2, confirming that g-C_3N_4–TiO_2 composites formed during pyrolysis. It is evident that the (002) diffraction peak for g-C_3N_4 overlaps with the (110) peak for the TiO_2 rutile phase. In comparison to the patterns for pure g-C_3N_4 and TiO_2, the g-C_3N_4 (002) peak is relatively weak and broad for g-C_3N_4–TiO_2-26 and is hardly detectable for g-C_3N_4–TiO_2-80. This can be attributed to the low g-C_3N_4 content; it is also possible that the g-C_3N_4 size along the *c*-axis decreases in the composites.

TGA curves for the samples are shown in Fig. 2. The weight of TiO_2 is almost unchanged in the temperature range 25–800 °C (Fig. 2a), while g-C_3N_4 exhibits a weight loss of <5% due to adsorbed water at 150 °C, and severe weight loss at temperatures higher than the decomposition temperature of 600 °C, with nearly 0% weight retained at 800 °C (Fig. 2e). However, the decomposition temperature of g-C_3N_4 decreases to ~512 °C for the composites (Fig. 2b–d), which indicates that TiO_2 has a catalytic effect on g-C_3N_4 decomposition. The residual weight for the

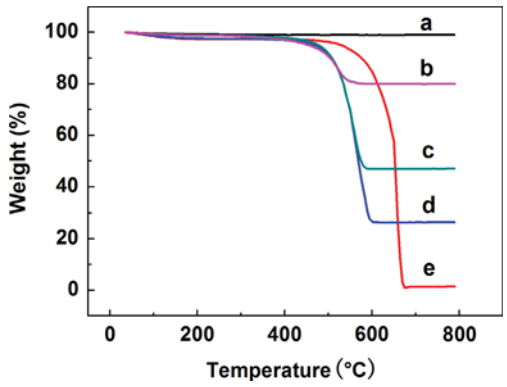

Fig. 2. Thermogravimetric analysis results for (a) TiO_2, (b) g-C_3N_4–TiO_2-80, (c) g-C_3N_4–TiO_2-47, (d) g-C_3N_4–TiO_2-26, and (e) g-C_3N_4.

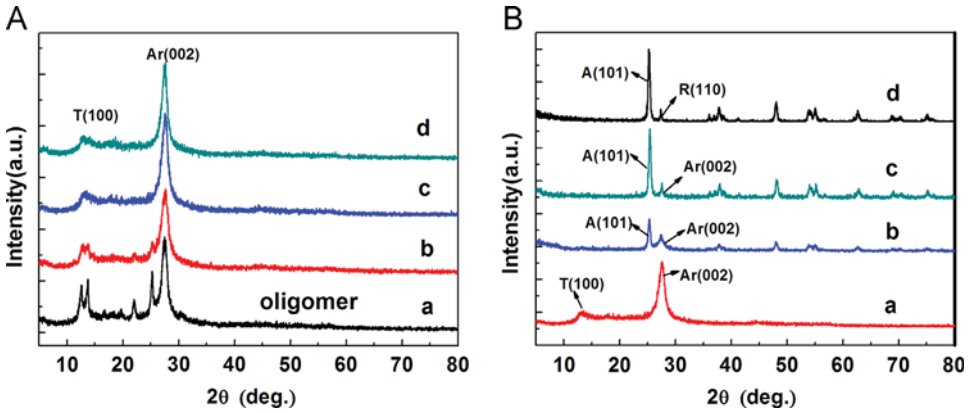

Fig. 1. XRD patterns for as-synthesized g-C_3N_4 samples and g-C_3N_4–TiO_2. (a) g-C_3N_4 prepared at 500 °C (curve a), 520 °C (curve b), 540 °C (curve c), and 560 °C (curve d). (b) g-C_3N_4 (curve a), g-C_3N_4–TiO_2-26 (curve b) and g-C_3N_4–TiO_2-80 (curve c) prepared at 540 °C, and TiO_2 (P25) (curve d). T, tri-s-triazine units; Ar, interlayer stacking of aromatic segments; A, anatase; R, rutile.

composites corresponds to their TiO_2 content. Thus, the TGA data indicate that the TiO_2 content is approximately 80.0% for g-C_3N_4–TiO_2-80, 46.9% for g-C_3N_4–TiO_2-47, and 26.4% for g-C_3N_4–TiO_2-26. It is notable that the g-C_3N_4 content in the composites as determined by TGA is consistent with the nominal content when g-C_3N_4 is the major component (> 50%) but is slightly lower than the nominal content when g-C_3N_4 is the minor component, which can be attributed to sublimation of melamine.

From the SEM images of g-C_3N_4, TiO_2, and g-C_3N_4–TiO_2 composites shown in Fig. S3, it is evident that the g-C_3N_4 and g-C_3N_4–TiO_2 samples exhibit a layered and plate-like surface morphology; however, more detailed information cannot be obtained from the SEM images. To investigate the sample microstructure, TEM images were recorded and are shown in Fig. 3. g-C_3N_4 exhibits a distinct sheet-like structure (Fig. 3a) with a wide sheet size distribution. The diameter of TiO_2 particles is approximately 25 nm and the material exhibits relatively good dispersion (Fig. 3b), although there are some aggregates among the particles. The TEM image of g-C_3N_4–TiO_2-26 in Fig. 3c confirms the coexistence of sheet-like g-C_3N_4 and TiO_2 particles, with the latter dispersed on the g-C_3N_4 surface. However, g-C_3N_4 sheets are not obvious in the TEM image of g-C_3N_4–TiO_2-80 (Fig. 3d). Comparison with the image for pure TiO_2 reveals that there are some layers coated on the surface of TiO_2 particles. The TEM images indicate that g-C_3N_4 can act as a support when the TiO_2 content in the composite is low, while TiO_2 particles can act as a substrate to disperse g-C_3N_4 when TiO_2 is the main component of the composite. The results are consistent with the XRD patterns, which reveals that the presence of TiO_2 in the composites may decrease the size of g-C_3N_4 along the *c*-axis.

To identify the valence state of elements in the samples, XPS spectra of g-C_3N_4, TiO_2 and g-C_3N_4–TiO_2 were recorded and are shown in Fig. 4. The results indicate that the g-C_3N_4–TiO_2 composites contain C, N, O, and Ti (Fig. 4a). The C/N ratio for g-C_3N_4 is 0.76, which is close to the theoretical value of 0.75. The C/N ratios of 0.69 for g-C_3N_4–TiO_2-26 and 0.68 for g-C_3N_4–TiO_2-80 are less than the theoretical value, which can be attributed to edge defects caused by uncondensed amino groups [35]. The g-C_3N_4 C/N ratio will decrease with increasing edge defects, which are related to the g-C_3N_4 size. High-resolution C 1s, N 1s, and Ti 2p XPS spectra are shown in Fig. 4b–d. The XPS peaks can be fitted using a Gauss–Lorentz shape after Shirley background correction. For example, the C 1s spectrum can be deconvoluted into four peaks located at 284.6 (C1), 286.2 (C2), 288.2 (C3), and 289.6 eV (C4). The peak at 284.6 eV is attributed to atoms in a pure carbon environment (C–C bonds), typically ascribed to graphitic carbon [17,34,36,37]. The peak at 286.2 eV can be assigned to C bonded to N, usually ascribed to defect-containing sp^2-hybridized carbon atoms present in graphitic domains [37–39]. The peak at 288.2 eV corresponds to sp^2-hybridized carbon in N=C–N_2, in which C is bonded to three neighboring N atoms via one double and two single bonds [40]. The peak at 289.6 eV can be assigned to C in O=C–OR. The g-C_3N_4–TiO_2 composites exhibit similar fitted C 1s peaks, indicating the existence of graphite-like carbon nitride. The N 1s spectra for g-C_3N_4 and g-C_3N_4–TiO_2 can be deconvoluted into three peaks located at 398.6 (N1), 399.8 (N2), and 400.9 eV (N3). The peak at 398.6 eV is assigned to pyridine-type N (C–N=C) [41–43]. The N2 peak is attributed to tertiary nitrogen (N–$(C)_3$) and the N3 peak to an amino group carrying a hydrogen atom, which might be related to structural defects and incomplete condensation during the polymerization process [44–46]. The C 1s and N 1s XPS data provide evidence of the existence of g-C_3N_4 in the composites. The Ti 2p XPS profile for g-C_3N_4–TiO_2 is similar to that for TiO_2, but the peaks are slightly shifted to lower binding energy compared with TiO_2, indicating that electron interaction transfer from g-C_3N_4 to Ti occurs, leading to an increase in the outer electron

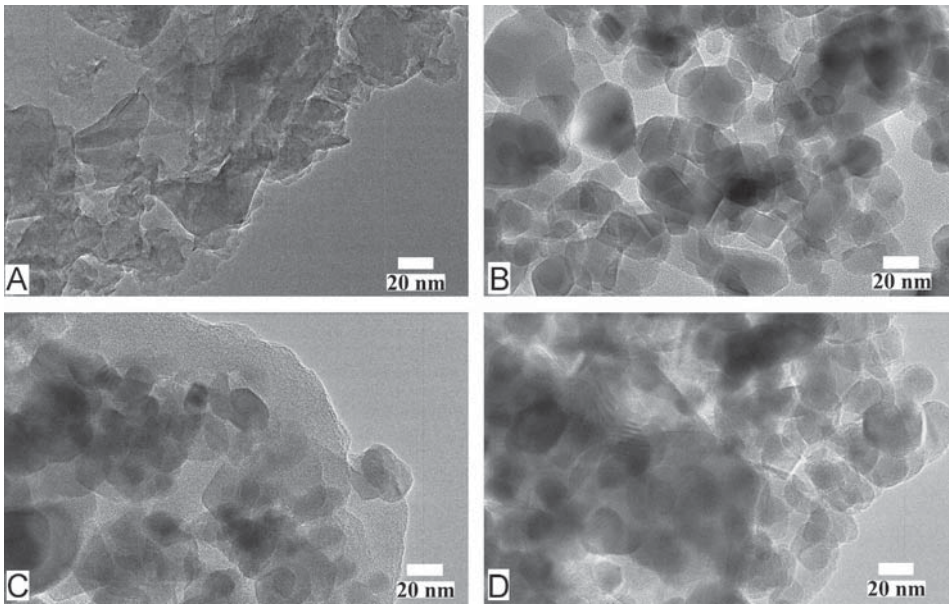

Fig. 3. TEM images of (a) g-C_3N_4, (b) TiO_2, (c) g-C_3N_4–TiO_2-26, and (d) g-C_3N_4–TiO_2-80.

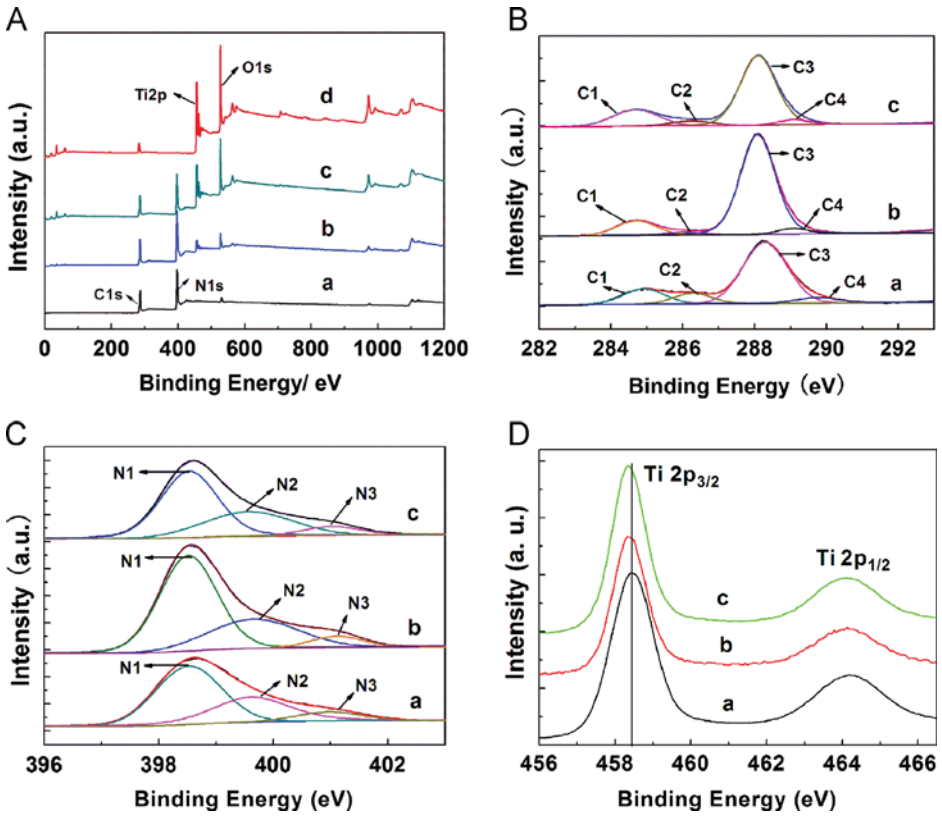

Fig. 4. (a) XPS survey spectra: curve a, g-C_3N_4; curve b, g-C_3N_4–TiO_2-26; curve c, g-C_3N_4–TiO_2-80; and curve d, TiO_2. High-resolution XPS (b) C 1s and (c) N 1s spectra: curve a, g-C_3N_4; curve b, g-C_3N_4–TiO_2-26; and curve c, g-C_3N_4–TiO_2-80. (d) XPS Ti 2p spectra: curve a, TiO_2; curve b, g-C_3N_4–TiO_2-26; and curve c, g-C_3N_4–TiO_2-80.

cloud density of Ti and a decrease in Ti 2p binding energy. This suggests that there is some intense interaction between TiO_2 and g-C_3N_4 species.

UV-visible diffuse reflectance spectra (DRS) for the samples are shown in Fig. 5a. TiO_2 has an absorption edge at ~400 nm, with strong absorption in the UV region and weak absorption in the range 400–800 nm (Fig. 5a curve a). g-C_3N_4 can absorb light at wavelengths up to 450 nm, but its absorption capacity in the UV range is weaker than that of TiO_2. After combining g-C_3N_4 with TiO_2, the absorbance edge of g-C_3N_4–TiO_2 composites obviously shifts to longer wavelength. It is interesting that g-C_3N_4–TiO_2-80 (Fig. 5a curve d) shows higher absorption in both the UV and visible regions than g-C_3N_4–TiO_2-26, which may indicate that this composite has high activity due to generation of more electron–hole pairs under visible light irradiation.

PLS data were measured to determine the migration, transfer, and recombination processes for photogenerated electron–hole pairs in the samples. The photocatalytic activity of catalysts depends on the separation efficiency for photo-induced electron–hole pairs: the higher the electron–hole separation efficiency, the higher are the photocurrent and catalytic activity. For excitation at 365 nm, g-C_3N_4 showed a strong emission peak at ~450 nm (Fig. 5b curve a), which can be attributed to band-to-band photoluminescence, because the light energy approximately equals the bandgap energy of g-C_3N_4 (2.73 eV), so electrons and holes can rapidly recombine [34]. The emission peak intensity is significantly lower for g-C_3N_4–TiO_2 composites (Fig. 5b, curves b and c), which indicates that the composites have much lower recombination rates and that TiO_2 introduction can inhibit electron–hole recombination. Furthermore, the emission peaks for g-C_3N_4–TiO_2 are shifted to shorter wavelength; for example, the peak position is 443 nm for g-C_3N_4–TiO_2-26 and 440 nm for g-C_3N_4–TiO_2-80. This indicates that the g-C_3N_4 bandgap has widened because the conjugated system has decreased in size owing to interactions between TiO_2 and g-C_3N_4.

3.2. Photodegradation characteristics

A pseudo-first-order reaction model can usually describe experimental data for photodegradation according to [47]

$$\ln \frac{C_0}{C_t} = K_{app}\, t, \tag{1}$$

where C_0 is the initial MB concentration, t is the reaction time, C_t is the MB concentration at reaction time t, and K_{app} is the apparent first-order rate constant. During degradation, the absorbance of MB in solution decreases with increasing irradiation time (Figs. S4 and S5), indicating that the dye has decomposed. The degradation capacity of g-C_3N_4 prepared at different temperatures was analyzed using a pseudo-first-order reaction model and the results are shown in Fig. 6a. The largest K_{app} value

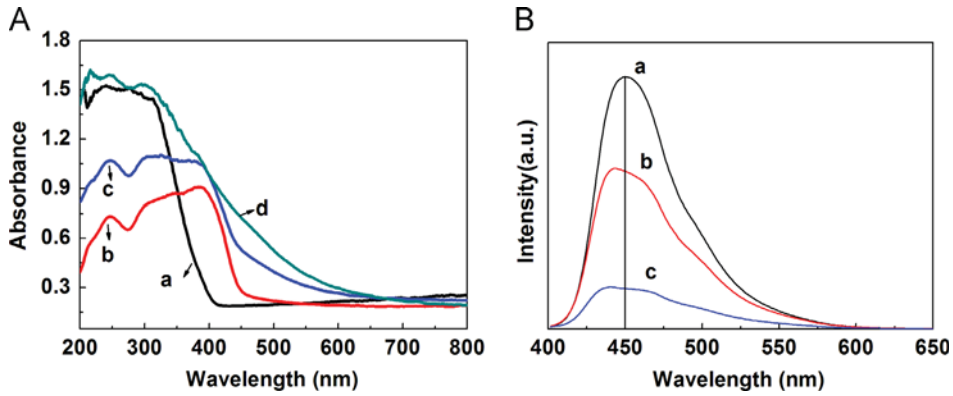

Fig. 5. (a) UV-visible diffuse reflectance spectra: curve a, TiO_2 (P25); curve b, g-C_3N_4; curve c, g-C_3N_4–TiO_2-26; and curve d, g-C_3N_4–TiO_2-80. (b) Photoluminescence spectra: curve a, g-C_3N_4; curve b, g-C_3N_4–TiO_2-26; and curve c, g-C_3N_4–TiO_2-80.

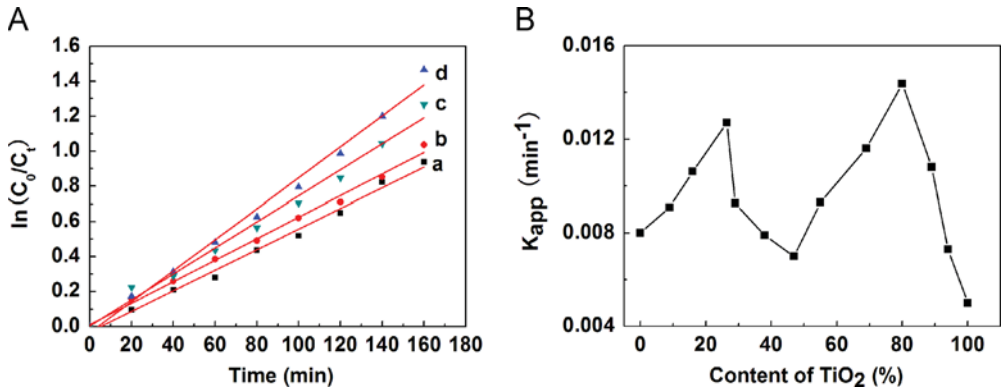

Fig. 6. (a) Kinetics of MB degradation under visible light irradiation over g-C_3N_4 prepared at pyrolysis temperatures of 500 °C (curve a), 520 °C (curve b), 560 °C (curve c), and 540 °C (curve d). (b) Relationship between the apparent rate K_{app} for MB degradation under visible light irradiation and the TiO_2 content in g-C_3N_4–TiO_2 composites prepared at 540 °C.

($\sim 8.83 \times 10^{-3}$ min^{-1}) is observed for g-C_3N_4 prepared at 540 °C (Fig. 6a). Therefore, g-C_3N_4–TiO_2 composites were prepared at the optimum temperature of 540 °C.

K_{app} for MB degradation over g-C_3N_4–TiO_2 composites first increased with the TiO_2 content up to 26.4%, then decreased for TiO_2 content up to ~47%, increased again with the TiO_2 content and reached a maximum for ~80% TiO_2, and decreased with further increases in the TiO_2 content (Fig. 6b). These results show that the g-C_3N_4–TiO_2-26 and g-C_3N_4–TiO_2-80 composites, which contain different amounts of TiO_2, exhibited good photocatalytic activity. The TEM and XRD results indicate that g-C_3N_4 can be used as a support when the TiO_2 content is low, while TiO_2 particles can act as a substrate to disperse g-C_3N_4 when TiO_2 is the major component. Both g-C_3N_4 and TiO_2 are semiconductors, so TiO_2 particles can act as modifiers that decorate g-C_3N_4 when the TiO_2 content is low, and g-C_3N_4 sheets can act as modifiers that decorate TiO_2 particles when the TiO_2 content is high. Regardless of whether g-C_3N_4 or TiO_2 is the major component, K_{app} for MB degradation exhibits maximal values for optimal component ratios in the composites. Thus, there is a zigzag relation between K_{app} and the TiO_2 content (Fig. 6b).

Control MB degradation experiments were carried out using radiation without a photocatalyst and without irradiation in the presence of a photocatalyst (Fig. S6). K_{app} for MB degradation is very low for control tests without light irradiation (6.41×10^{-4} min^{-1}) and without a photocatalyst (1.49×10^{-3} min^{-1}). In comparison, K_{app} for MB degradation on g-C_3N_4–TiO_2-80 under light irradiation is much greater, which clearly demonstrates that MB removal can be attributed to degradation rather than an adsorption mechanism.

MB photodegradation rates over selected samples are shown in Fig. 7a. For example, the MB degradation rate at 160 min was ~55% for TiO_2 and 76% for g-C_3N_4 as catalysts. TiO_2 shows low photocatalytic performance because of poor visible light absorption owing to its large bandgap (3.16 eV). The MB removal efficiency was ~89% on g-C_3N_4–TiO_2-26 and ~92% on g-C_3N_4–TiO_2-80 at 160 min, both of which are higher in comparison to g-C_3N_4 and TiO_2. This might be attributable to good dispersion of TiO_2 on g-C_3N_4 or of g-C_3N_4 on TiO_2, resulting in maximization of interfaces between the two semiconductors and the highest efficiency for charge carrier separation. Fig. 7b shows the corresponding pseudo-first-order kinetics plot for the samples. Under the same experimental conditions, K_{app} values for MB degradation on g-C_3N_4–TiO_2-26 (1.27×10^{-2} min^{-1}) and g-C_3N_4–TiO_2-80 (1.44×10^{-2} min^{-1}) are greater than for g-C_3N_4 (8.08×10^{-3} min^{-1}) and TiO_2 (5.10×10^{-3} min^{-1}). The results clearly demonstrate that photocatalytic performance can be enhanced by the formation of g-C_3N_4–TiO_2 composites.

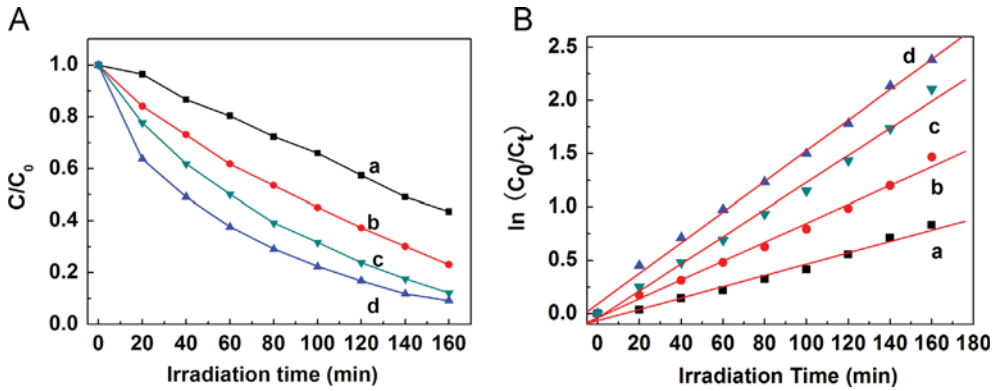

Fig. 7. (a) MB photodegradation under visible light irradiation and (b) first-order kinetics plot: curve a, g-C_3N_4; curve b, g-C_3N_4–TiO_2-26; curve c; and curve d, g-C_3N_4–TiO_2-80.

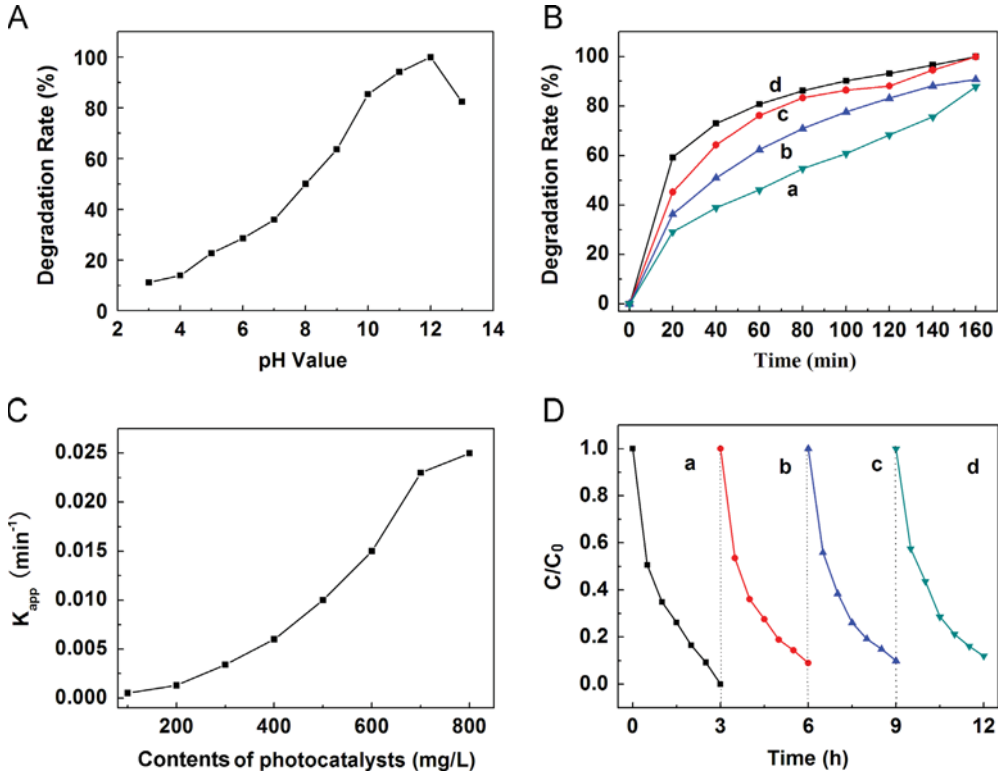

Fig. 8. (a) Effect of pH on the rate of MB photodegradation. (b) Effect of initial MB concentration on the photocatalytic activity of g-C_3N_4–TiO_2-80: curve a, 25 mg L^{-1}; curve b, 20 mg L^{-1}; curve c, 10 mg L^{-1}; and curve d, 5 mg L^{-1}. (c) Relationship between K_{app} for MB degradation and g-C_3N_4–TiO_2-80 concentration. (d) Consecutive MB degradation runs using the same g-C_3N_4–TiO_2-80 sample under visible light irradiation: curve a, first run; curve b, second run; curve c, third run; and curve d, fourth run.

The scheme for photogenerated electron–hole separation in the g-C_3N_4–TiO_2 composite shown in Fig. S7 can be discussed as follows. The conduction band (CB) and valence band (VB) edge potentials are at approximately −1.12 and 1.57 eV for g-C_3N_4 and at approximately −0.29 and 2.91 eV for TiO_2, respectively [25]. When the system is irradiated with visible light, only g-C_3N_4 can absorb visible light and be excited. In g-C_3N_4, photogenerated electrons are excited from the VB to the CB, resulting in holes (h^+) in the VB. Photogenerated electrons on the g-C_3N_4 surface can easily transfer to the CB of TiO_2, while photogenerated h^+ migrate to the g-C_3N_4 surface in the composite. This effective separation of photogenerated electron–hole pairs enhances the photodegradation performance.

The effect of pH on the MB degradation efficiency was studied in the pH range 3–13 [48–50]. The g-C_3N_4–TiO_2-80 concentration was kept at 200 mg L^{-1} for a reaction time of 30 min at room temperature and an MB concentration of 20 mg L^{-1} (50 mL). The rate of MB photodegradation on g-C_3N_4–TiO_2-80 at different pH values is shown in Fig. 8a. It is clear that the rate of MB degradation increases with pH and reaches approximately 100% at pH 12. This may be

because a change in pH affects the adsorption behavior of MB which bears positive ion on the surface of photocatalyst where more negative charges has carried at high pH [50]. Another reason may be that OH^- can act as a capture agent for h^+, which generates $\cdot OH$, so an increase in pH reduces the recombination probability for photogenerated electrons and holes, which enhances the photocatalytic activity. However, when the solution pH is greater than 12, the rate of MB photodegradation obviously decreases. This is because of competition between OH^- and MB for adsorption sites on the composite surface [50].

The effect of the MB concentration on photocatalytic activity was also investigated (Fig. 8b). The rate of MB degradation decreased with increasing initial MB concentration. The reason for this behavior is that excess dye molecules decrease the number of active sites on the photocatalyst; moreover, excess dye molecules absorb light and thus reduce the number of photons that reach the photocatalyst surface [48]. K_{app} for MB photodegradation increased relatively quickly with catalyst concentration in the range 100–700 mg L^{-1}, but relatively slowly when the concentration of catalyst was larger than 700 mg L^{-1}. The results indicate that the catalyst does not absorb the light completely at low concentrations, so K_{app} increases with the catalyst concentration up to700 mg L^{-1}. However, K_{app} then decreases with further increases in the catalyst concentration because incident light may be reflected by excess catalyst particles [50].

3.3. Stability of g-C_3N_4–TiO_2-80

Besides activity, stability is also important for practical application of photocatalysts. Therefore, reuse of g-C_3N_4–TiO_2-80 for MB photodegradation under visible light irradiation was investigated to evaluate the optical stability of the catalyst. The results are shown in Fig. 8d. The g-C_3N_4–TiO_2-80 sample used in four consecutive photodegradation runs showed a loss of catalytic activity of only 9.0%. Therefore, g-C_3N_4–TiO_2-80 may be relatively photostable during photocatalytic MB degradation.

4. Conclusion

g-C_3N_4–TiO_2 composites were synthesized by directly heating melamine and TiO_2 in a semi-closed system. Composites prepared at 540 °C with TiO_2 content of 26.4 and 80.0 wt% showed good photocatalytic activity for MB degradation. The enhanced catalytic capability is mainly due to effective separation of photogenerated carriers and wide optical absorption up to the visible-light region owing to the formation of the heterojunction from g-C_3N_4 and TiO_2. The g-C_3N_4–TiO_2-80 sample was robust and could be used for at least four runs with an activity loss of only 9%. Thus, the g-C_3N_4–TiO_2 composites described here may be prospective candidates for solving critical environmental and energy issues.

Acknowledgments

We appreciate funding from National Natural Science Foundation of China (21274082 and 21073115), the Natural Science Foundation of Shanxi Province (2014011016-1) and Program for New Century Excellent Talents in University (NCET-10-0926).

Appendix A. Supporting information

Supplementary data associated with this article can be found in the online version at http://dx.doi.org/10.1016/j.mssp.2014.08.004.

References

[1] I. Nakamura, N. Negishi, S. Kutsuna, T. Ihara, S. Sugihara, K. Takeuchi, J. Mol. Catal. A Chem. 161 (2000) 205–212.
[2] M.R. Hoffmann, S.T. Martin, W.Y. Choi, D.W. Bahnemann, Chem. Rev. 95 (1995) 69–96.
[3] H. Benhebal, M. Chaib, A. Leonard, S.D. Lambert, M. Crine, Mater. Sci. Semicond. Process. 15 (2012) 264–269.
[4] Q.Z. Wang, J. Hui, Y.J. Huang, Y.M. Ding, Y.X. Cai, S.Q. Yin, Z.M. Li, B.T. Su, Mater. Sci. Semicond. Process. 17 (2014) 87–93.
[5] F. Spadavecchia, G. Cappelletti, S. Ardizzone, C.L. Bianchi, S. Cappelli, C. Oliva, P. Scardi, M. Leoni, P. Fermo, Appl. Catal. B Environ. 96 (2010) 314–322.
[6] J.H. Sun, S.Y. Dong, Y.K. Wang, S.P. Sun, J. Hazard. Mater. 172 (2009) 1520–1526.
[7] A. Linsebigler, G. Lu, J. Yates Jr., Chem. Rev. 95 (1995) 735–758.
[8] E. Borgarello, J. Kiwi, E. Pelizzetti, M. Visca, M. Gratzel, Nature 289 (1981) 158–160.
[9] J. Moon, C.Y. Yun, K.W. Chung, M.S. Kang, J. Yi, Catal. Today 87 (2003) 77–86.
[10] R. Asahi, T. Morikawa, T. Ohwaki, K. Aoki, Y. Taga, Science 293 (2001) 269–271.
[11] F.B. Li, X.Z. Li, Chemosphere 48 (2002) 1103–1111.
[12] K.Y. Jung, S.B. Park, S.K. Ihm, Appl. Catal. B Environ. 51 (2004) 239–245.
[13] F.Z. Su, S.C. Mathew, G. Lipner, J. Am. Chem. Soc. 132 (2010) 16299–16301.
[14] Y.J. Zhang, T. Mori, J.H. Ye, J. Am. Chem. Soc. 132 (2010) 6294–6295.
[15] G.Z. Liao, S. Chen, X. Quan, J. Mater. Chem. 22 (2012) 2721–2726.
[16] S.C. Yan, Z.S. Li, Z.G. Zou, Langmuir 25 (2009) 10397–10401.
[17] S.C. Yan, S.B. Lv, Z.S. Li, Z.G. Zou, Dalton Trans. 39 (2010) 1488–1491.
[18] X.C. Wang, K. Maeda, A. Thomas, K. Takanabe, G. Xin, J.M. Carlsson, K. Domen, M. Antonietti, Nat. Mater. 8 (2009) 76–80.
[19] Y. Sakataa, K. Yoshimoto, K. Kawaguchia, H. Imamura, S. Higashimoto, Catal. Today 161 (2011) 41–45.
[20] Y. Di, X.C. Wang, A. Thomas, A. Antonietti, ChemCatChem 2 (2010) 834–838.
[21] G. Liu, P. Niu, C. Sun, S.C. Smith, Z. Chen, G.Q. Lu, H.M. Cheng, J. Am. Chem. Soc. 132 (2010) 11642–11648.
[22] X.F. Chen, J.S. Zhang, X.Z. Fu, J. Am. Chem. Soc. 131 (2009) 1165–1169.
[23] H.J. Yan, H. Yan, Chem. Commun. 47 (2011) 4168–4170.
[24] J.X. Sun, Y.P. Yuan, L.G. Qiu, X. Jiang, A.J. Xie, Y.H. Shen, J.F. Zhu, Dalton Trans. 41 (2012) 6756–6763.
[25] S.S. Zhao, S. Chen, H.T. Yu, X. Quan, Sep. Purif. Technol. 99 (2012) 50–54.
[26] C. Miranda, H. Mansilla, J. Yánez, S. Obregón, G. Colón, J. Photochem. Photobiol. A 253 (2013) 16–21.
[27] X.F. Lu, Q.L. Wang, D.L. Cui, J. Mater. Sci. Technol. 26 (2010) 925–930.
[28] N. Yang, G.Q. Li, W.L. Wang, X.L. Yang, W.F. Zhang, J. Phys. Chem. Solids 72 (2011) 1319–1324.
[29] H.J. Yan, H.X. Yang, J. Alloys Cmpd. 509 (2011) L26–L29.
[30] S.Q. Zhang, Y.X. Yang, Y.N. Guo, W. Guo, M. Wang, Y.H. Guo, M.X. Huo, J. Hazard. Mater. 261 (2013) 235–245.
[31] K. Katsumata, R. Motoyoshi, N. Matsushita, K. Okada, J. Hazard. Mater. 260 (2013) 475–482.
[32] W. Ruland, B.M. Smarsly, J. Appl. Crystallogr. 40 (2007) 409–417.
[33] M. Kawaguchi, K. Nozaki, Chem. Mater. 7 (1995) 257–264.
[34] A. Thomas, A. Fischer, F. Goettmann, M. Antonietti, J.O. Muller, R. Schlogl, J.M. Carlsson, J. Mater. Chem. 18 (2008) 4893–4908.
[35] F. Goettmann, A. Fischer, M. Antonietti, A. Thomas, Angew. Chem. Int. Ed. 45 (2006) 4467–4471.
[36] X. Wang, X. Chen, A. Thomas, X. Fu, M. Antonietti, Adv. Mater. 21 (2009) 1609–1612.

[37] D. Matton, K.J. Boyd, A.H. Al-Bayati, S.S. Todorov, J.W. Rabalais, Phys. Rev. Lett. 73 (1994) 118–121.
[38] Q.J. Xiang, J.G. Yu, M. Jaroniec, J. Phys. Chem. C 115 (2011) 7355–7363.
[39] V.N. Khabashesku, J.L. Zimmerman, J.L. Margrave, Chem. Mater. 12 (2000) 3264–3270.
[40] Q.X. Guo, Y. Xie, X.J. Wang, S.Y. Zhang, T. Hou, S.C. Lv, Chem. Commun. (2004) 26–27.
[41] C. Palacio, C. Gomez-Aleixandre, D. Diaz, M.M. Garcia, Vacuum 48 (1997) 709–713.
[42] B. Angleraud, N. Mubumbila, P.Y. Tessier, V. Fernandez, G. Turban, Diamond Relat. Mater. 10 (2001) 1142–1146.
[43] Y.G. Li, J.A. Zhang, Q.S. Wang, Y.X. Jin, D.H. Huang, Q.L. Cui, G.T. Zou, J. Phys. Chem. B 114 (2010) 9429–9434.
[44] S. Bhattacharyya, C. Cardinaud, G. Turban, J. Appl. Phys. 83 (1998) 4491–4499.
[45] S. Bhattacharyya, J. Hong, G. Turban, J. Appl. Phys. 83 (1998) 3917–3919.
[46] Z.X. Ding, X.F. Chen, M. Antonietti, X.C. Wang, ChemSusChem 4 (2011) 274–281.
[47] F.F. Yang, G.Y. Han, D.Y. Fu, Y.Z. Chang, H.F. Wang, Mater. Chem. Phys. 140 (2013) 398–404.
[48] H.R. Rajabi, O. Khani, M. Shamsipur, V. Vatanpour, J. Hazard. Mater. 250–251 (2013) 370–378.
[49] M. Shamsipur, H.R. Rajabi, O. Khani, Mater. Sci. Semicond. Process. 16 (2013) 1154–1161.
[50] D.Y. Fu, G.Y. Han, Y.Z. Chang, J.H. Dong, Mater. Chem. Phys. 132 (2012) 673–681.